Using phased array beamforming to identify broadband noise sources in a turbofan engine

Pieter Sijtsma
Senior Scientist, National Aerospace Laboratory NLR
P.O. Box 153, 8300 AD, Emmeloord, The Netherlands
sijtsma@nlr.nl

Fan broadband noise is a major component of the total noise emitted by turbofan engines, especially at lower shaft speeds. It is generated in the rotor/stator region, but the exact origin is not always known. This article discusses the application of phased array beamforming techniques for a better understanding of the source mechanisms of fan broadband noise. The Conventional Beamforming technique was applied, as well as the deconvolution technique CLEAN-SC and the beamforming technique ROSI for rotating sources. Beamforming was applied to acoustic data measured by two circular microphone arrays that were mounted in the intake and in the bypass of a Rolls-Royce fan rig. These arrays are normally used for the detection of azimuthal modes. The merits of beamforming are discussed by considering a number of typical low shaft speed cases. Using the intake array, in one of the cases forward radiating broadband noise sources were found that were coherent over a large area. These could have been due to a rotor instability. In an other case, the forward radiating broadband noise seemed to have its origin at the stator vanes. This could be made plausible with the help of the intake mode detection results. Using the bypass array, stator bound noise sources were found that seemed to be distributed along the span of the vanes. In other words, tip sources seemed to be of minor importance for aft radiating fan broadband noise. The bypass mode detection results seemed to indicate that the spanwise distributed noise sources were located at the trailing edges of the stator vanes.

NOMENCLATURE

BPF	Blade Passing Frequency
CB	Conventional Beamforming
CLEAN-SC	CLEAN based on Spatial source Coherence
LE	Leading Edge
ROSI	ROtating Source Identifier
RPM	Revolutions Per Minute
TE	Trailing Edge
A	source power
B	number of rotor blades
$\mathbf{C}$	Cross-Spectral Matrix
c	speed of sound
$\vec{e}_x$	unit vector in x-direction
F	transfer function
f	frequency
f_{sam}	sample frequency
G	Green's function
$\mathbf{g}$	steering vector
i	imaginary unit
$\mathcal{J}$	cost function
j	engine order
k	azimuthal mode number
l	revolution index
M	Mach number of uniform axial flow
m	microphone index
N	number of microphones
n	microphone index
p	Fourier component of acoustic pressure
r	radial position
S	subset of all possible (m,n)-combinations
$S_{k\mu}(r)$	shielded fraction
t	time (at receiver)
U	speed of uniform axial flow
$\vec{x}$	receiver position, (x, y, z)
x_{TE}	axial position of rotor blade LE
x_{LE}	axial position of rotor blade TE
α_{km}	axial wave number
β^2	$1-M^2$
$\chi(t)$	measured acoustic pressure
Δt_e	emission time delay

ϕ_l	pulse time
μ	radial mode number,
v	sample index
$\sigma(t)$	source signal
τ	time (at source)
$\vec{\xi}$	source position, (ξ, η, ζ)
Ω	shaft frequency

1. INTRODUCTION

Through better design and the use of higher bypass ratios, aircraft turbofan engine noise has been substantially reduced over the last decades. As a consequence, on modern aircraft many other noise sources, like slats, flaps, and landing gears, have comparable strengths. Nevertheless, even in the landing phase, the engines are usually still the loudest noise sources1. Hence, there is a continuous need for further reducing engine noise.

Engine noise can be either tonal (buzz-saw noise, rotor alone noise, rotor-stator interaction, blade row interaction in the turbine) or broadband (jet noise, fan broadband noise). Tonal sound and jet noise have been extensively studied since many years, which has led to significant noise reduction. As a consequence, the relative contribution of fan broadband noise is increasing, and is therefore becoming a more and more important topic of research[2].

Especially at lower shaft speeds, typically during approach, fan broadband noise is a major component of the total noise emitted by turbofan engines. This broadband noise can be caused by various possible mechanisms: interaction of the intake duct boundary layer with the rotor blade tips, interaction of the turbulent rotor wakes with the stator vanes, rotor blade self noise (trailing edge noise), and stator vane self noise.

For investigations of broadband noise reduction devices it is important to know which of the above-mentioned source mechanisms prevail. Unfortunately, there is no straightforward recipe to locate these sources experimentally, and to estimate their strengths. An interesting experimental study to determine a ranking of different broadband noise source mechanisms on a fan rig was performed by Moreau and Enghardt[3]. They varied the rotor-stator gap, the stator vane count, and the inflow turbulence levels in order to distinguish between the various rotor-stator interaction mechanisms. A more direct approach of finding the dominant sources may be the phased array beamforming technique[4], which has become a standard tool for acoustic source location in wind tunnel and flight testing.

The application of phased array beamforming inside turbofan engines is still in its infancy. The feasibility to locate sources on rotor blades and stator vanes of a fan rig was demonstrated recently by Sijtsma[5,6]. This was done with an existing intake circular microphone array, which is normally used for azimuthal mode detection. By Conventional Beamforming, sources could be made visible on the stator. Moreover, using beamforming with rotating focus, sources were visualized on the rotor.

The above-mentioned application of in-duct beamforming makes use of free-field Green's functions to construct the so-called "steering vectors". This means that wall-reflections were ignored. To reduce the effects of these reflections, the measurements were carried out with an intake liner. A different beamforming approach was followed by Lowis and Joseph[7], who included duct wall reflections in the Green's function. Recently, Dougherty and Walker[8] applied steering vectors based on unsteady rotor blade pressures, instead of using Green's functions.

This article describes the actual status of in-duct beamforming. In

Section 2 the techniques are discussed, and Section 3 considers a number of typical applications. The contents of this article are partly extracted from earlier publications[5,6]. New in this article is the application of beamforming to a microphone array in the bypass duct. Moreover, the added value is shown of using beamforming in combination with azimuthal mode detection.

2. BEAMFORMING

Phased array beamforming techniques make use of a theoretical model for the sound transfer from source to receiver. In traditional applications, where the microphone array is at a certain distance from the model, the free-field Green's function (with optionally a uniform flow) is used for that purpose. Inside a duct this might not be the most appropriate choice, because reflections of the duct wall are not included. It may be better to use numerically calculated Green's functions which include the presence of the nacelle. Even measured Green's functions may be used. Nonetheless, inaccuracies will remain, because these Green's functions do not include the (often unknown) source directivities. In this article we simply use the free-field Green's function, hence wall reflections are neglected.

2.1. STATOR BEAMFORMING

The most straightforward way to process phased array data is the Conventional Beamforming (CB) technique. This is a frequency-domain method, in which sound powers A of sources in points $\vec{\xi}$ on a scan plane are determined as follows. Let N be the number of microphones, and $\mathbf{C}$ the measured $N\times N$ cross-spectral matrix. Further, let $\mathbf{g}$ be the N-dimensional steering vector, which consists of simulated complex pressure amplitudes g_n at the microphone positions x_n, induced by a unit point source in $\vec{\xi}$. If S is a subset of all possible (m,n)-combinations, where m and n are microphone indices, then the source power A can be obtained through minimization of

$$J = \sum_{(m,n)\in S} \left| C_{mn} - A g_m g_n^* \right|^2, \qquad (1)$$

where the asterisk denotes complex conjugation. The solution is

$$A = \sum_{(m,n)\in S} g_m^* C_{mn} g_n \Big/ \sum_{(m,n)\in S} \left|g_m\right|^2 \left|g_n\right|^2. \qquad (2)$$

The steering vector components are usually Green's function values:

$$g_n = G\left(\vec{x}_n, \vec{\xi}\right). \qquad (3)$$

Using a Cartesian co-ordinate system (x, y, z), with the x-axis coinciding with the engine axis, the free-field Green's function is expressed as

$$G\left(\vec{x},\vec{\xi}\right) = \frac{\exp\left[-2\pi i f \Delta t_e\right]}{4\pi\sqrt{(x-\xi)^2 + \beta^2\left\{(y-\eta)^2 + (z-\zeta)^2\right\}}}. \qquad (4)$$

Herein, f is the frequency, and

$$\beta^2 = 1 - M^2, \qquad (5)$$

where M is the Mach number of the (assumed) uniform axial flow. Furthermore, we have in Eq. (4) the emission time delay:

$$\Delta t_e\left(\vec{x},\vec{\xi}\right) = \frac{1}{c\beta^2}\left(-M(x-\xi) + \sqrt{(x-\xi)^2 + \beta^2\left\{(y-\eta)^2 + (z-\zeta)^2\right\}}\right), \qquad (6)$$

where c is the sound speed.

Except for CB, which is summarized by Eq. (2), we will also use the deconvolution technique CLEAN-

SC (CLEAN based on Spatial source Coherence)[9].

2.2. ROTOR BEAMFORMING

To locate sources on the rotor we use the "rotating beamformer" ROSI (ROtating Source Identifier)[10], which is a time-domain beamforming technique. ROSI was applied earlier to rotating blades of wind turbines[11], and to helicopters[12]. A summary is given below.

With moving sources, it is in general not possible to apply frequency-domain beamforming techniques, because of the effects of the Doppler frequency shift. Instead of reconstructing source amplitudes at given frequencies, we have to reconstruct directly the signal $s(t)$ emitted by the source. For a source at moving position $\vec{\xi}(t)$ the free-field Green's function can be written as

$$G(\vec{x},\vec{\xi}(\tau),t,\tau)=\sigma(\tau)\Big/F\left(\vec{x},\vec{\xi}(\tau),t,\tau\right). \quad (7)$$

Herein, τ is the source time and t is the receiver time. The transfer function F is given by[10]

$$F\left(\vec{x},\vec{\xi}(\tau),t,\tau\right)=4\pi c\left\{\Delta t_e+\frac{1}{c^2}\left(-\vec{\xi}'(\tau)+U\vec{e}_x\right)\cdot\left(\vec{x}-\vec{\xi}(\tau)-U\Delta t_e\vec{e}_x\right)\right\} \quad (8)$$

in which the prime indicates the time derivative. Further, $U=Mc$ is the speed of the axial flow, and

$$\Delta t_e\left(\vec{x},\vec{\xi}(\tau)\right)=t-\tau=\frac{1}{c\beta^2}\left(-M\left(x-\xi(\tau)\right)+\sqrt{\left(x-\xi(\tau)\right)^2+\beta^2\left\{\left(y-\eta(\tau)\right)^2+\left(z-\zeta(\tau)\right)^2\right\}}\right). \quad (9)$$

If $\chi_n(t)$ is the acoustic pressure measured by the n-th microphone, then $\sigma(\tau)$ can be reconstructed by the "delay-and-sum" method:

$$\sigma(\tau)=\frac{1}{N}\sum_{n=1}^{N}\sigma_n(\tau), \quad (10)$$

where

$$\sigma_n(\tau)=\chi_n(t_n)F\left(\vec{x}_n,\vec{\xi}(\tau),t_n,\tau\right), \quad (11)$$

in which

$$t_n=\tau+\Delta t_e\left(\vec{x}_n,\vec{\xi}(\tau)\right). \quad (12)$$

Note that the receiver times t_n generally do not coincide with sample times. In that case $\chi_n(t)$ is linearly interpolated between two adjacent sample times. Source powers in the frequency domain can be obtained through Fourier transformation of $\sigma(\tau)$, and averaging:

$$A=\frac{1}{2}\sum_{n,m\in S}\left\langle\hat{\sigma}_n\hat{\sigma}_m^*\right\rangle\Big/\sum_{n,m\in S}1. \quad (13)$$

2.3. SUBTRACTION OF ROTOR BOUND TONES

Part of the acoustic signal measured by the microphones is repeated every rotor revolution. If the shaft speed is constant, then this "rotor-bound" sound consists of pure tones, at multiples of the shaft frequency. At low shaft speeds, when the rotor tip speed is subsonic, usually only the Blade Passing Frequency (BPF) and its higher harmonics appear. This article considers beamforming applications to the noise that is obtained after subtraction of the rotor tones from the total noise. In the following, this noise is called "broadband noise", even though it may contain tones that are not rotor-bound.

If a 1/rev pulse generator exists, the tones can be subtracted by the following "phase-locked averaging" method. Let

$$\chi\left(t_v\right)=\chi\left(v/f_{\text{sam}}\right) \quad (14)$$

be the sampled values of the acoustic

signal measured by one of the microphones. Consider a series of samples between two successive pulse times ϕ_{l-1} and ϕ_l:

$$\phi_{l-1} \le t_{v_{\min}} < t_{v_{\min}+1} < \ldots < t_{v_{\max}} < \phi_l. \quad (15)$$

Fourier components, per engine order j (multiple of the shaft frequency Ω), are calculated by:

$$p_j = \frac{2}{v_{\max} - v_{\min} + 1} \sum_{v=v_{\min}}^{v_{\max}} \chi(t_v) \exp \left[-2\pi i j (t_v - \phi_{l-1})/(\phi_l - \phi_{l-1})\right]. \quad (16)$$

The Fourier components are averaged over all revolutions l, and then calculated back to the time-domain:

$$\chi_{\text{tonal}}(t_v) = \sum_{j=1}^{(v_{\max}-v_{\min}+1)/2} p_j \exp \left[2\pi i j (t_v - \phi_{l-1})/(\phi_l - \phi_{l-1})\right]. \quad (17)$$

After subtraction of (17) from the acoustic signal, "broadband noise" remains.

3. APPLICATIONS

3.1. SET-UP

The beamforming techniques described in the previous chapter were applied to a few tests performed in the AneCom AeroTest facility on Rolls-Royce fan rigs. Figure 1 shows a drawing of the fan rig. The internal diameter is approximately 80 cm. Two microphone arrays were installed. The first one was located in the (drooped) intake, about 40 cm ahead of the leading edge (LE) of the rotor. To suppress nacelle wall reflections, a liner was installed between the rotor and the array. The second array was located in the outer surface of the bypass duct, approximately 15 cm downstream of the trailing edge (TE) of the stator. There was no liner between the stator and the bypass array. The arrays, each of which consisted of 100 Kulite sensors, were designed for azimuthal mode detection. They have non-uniform lay-outs, in order to be able to detect a large range of modes[13].

It is noted that a ring-shaped array is not ideal for beamforming. The beamforming results provide practically no resolution in axial direction. Beamforming on scan planes at different axial locations show the same acoustic sources, only their radial

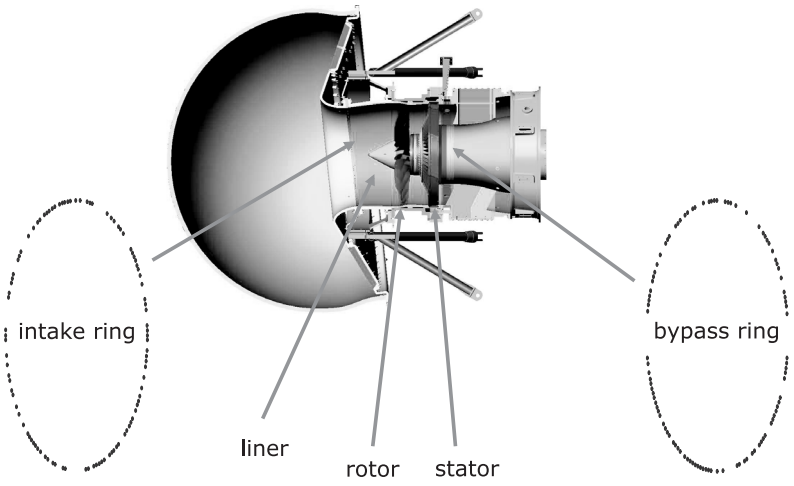

Figure 1: Drawing of the fan rig.

positions may vary. Sijtsma[6] showed that better beamforming results can be obtained by applying a "cage" array consisting of a number of parallel rings.

Beamforming results were obtained using disc-shaped scan planes aligned with the LE or the TE of the stator and the rotor. The stator results were obtained with CB, the rotor results with ROSI. The stator grid had a resolution of 0.5 cm, the resolution of the rotor grid was 1 cm. The rotor grid was coarser than the stator grid, because of the long computation times needed for ROSI. The stator grid was skewed in order to be aligned with the sweep of the stator vanes. The axial locations of the scan planes were according to the table below.

Array	*Method*	*Scan Plane*
intake	CB	stator LE
intake	ROSI	rotor LE
bypass	CB	stator TE

Results are presented of beamforming with "diagonal removal", i.e. the set S in Eqs. (2) and (13) consisted of all m,n-combinations, except $m=n$. Anyhow, the difference between the results of processing with and without diagonal was small. Beamforming results (after subtraction of the rotor tones) were calculated for each engine order individually. Afterwards, the results were summed up to 1/3 octave bands. Results are given for frequency bands ranging from 2500 Hz to 8000 Hz.

3.2. INTAKE ARRAY MEASUREMENTS OF 2005

First, results are presented from rig measurements that were carried out in 2005. During those tests, there were 24 rotor blades and 52 stator vanes. A typical low shaft speed case is considered: 4694 RPM, which is approximately 50% of the maximum speed. Intake CB and ROSI results are plotted in Figure 2 and Figure 3, respectively. The inner and outer surfaces of the bypass duct are indicated by the black circles. The maximum of each source map is adjusted to zero, and the range of the color scale is always 8 dB. The asymmetry in Figure 2 can probably be related to the asymmetric in-flow in the drooped intake.

In these images, not many details are visible. The CB images show some details in the 4000 Hz frequency band, though the spacing between the source spots seems to be too large to be associated with the stator vanes. In the ROSI images, the rotor blades are vaguely visible in the frequency bands of 3150 Hz and 4000 Hz. It appeared that the details in the 4000 Hz CB image were related to a spectral "hump". See Figure 4, which shows the narrow-band peak values of CB and ROSI. The maximum value of the hump in the CB results appeared at 4068 Hz. This frequency corresponds to engine order 52, which is not a multiple of the BPF*.

Additional information could be obtained from the azimuthal mode spectrum at this frequency, which is shown in Figure 5. It features a peak at mode number $k = 15$. In the rotating frame of reference, the $k = 15$ mode at $f = 52\Omega$ is experienced at $f = 37\ \Omega = 2894$ Hz. This frequency is the peak of a local hump in the ROSI results of Figure 4. The ROSI narrow-band result at 2894 Hz is shown in Figure 6. Now the 24 rotor blades can be recognized clearly. It is likely that the stator source at 4068 Hz and the rotor source at 2894 Hz were linked to each other through rotor-stator interaction[14], though the actual sources could be on either the rotor or the stator.

More information about the acoustic sources was gained with the beamforming technique CLEAN-SC, which is an iterative deconvolution method based on spatial source coherence[9]. By applying one iteration of CLEAN-SC, all sources that are coherent

*Actually, 52 was the number of stator vanes in 2005. It is not clear if there is any relation with the hump observed.

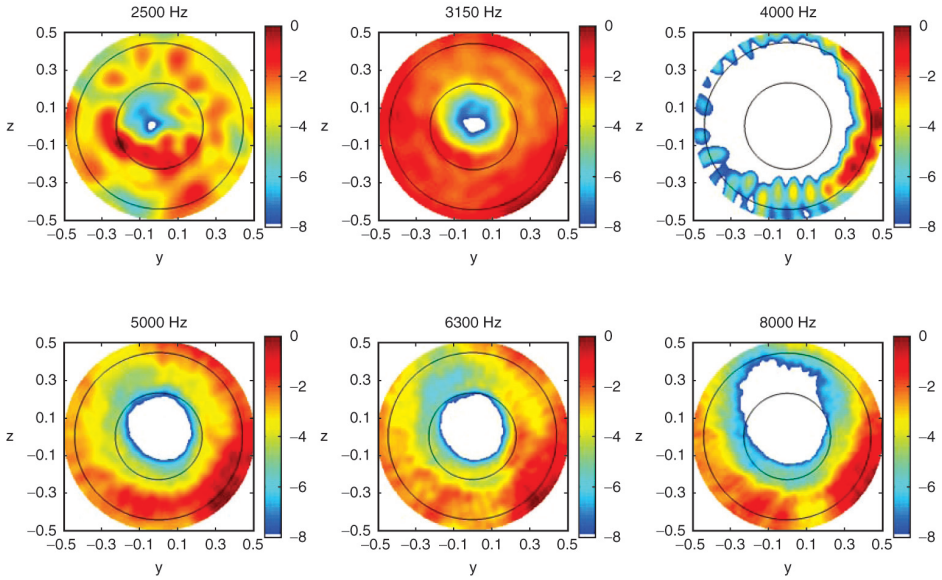

Figure 2: Intake array CB images on stator LE plane; 2005 fan rig measurements; 4694 RPM.

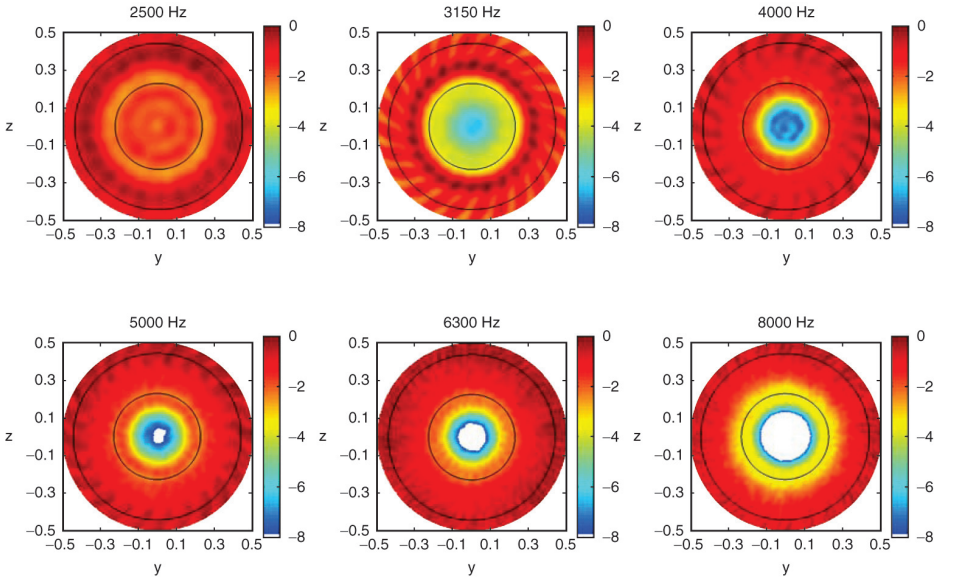

Figure 3: Intake array ROSI images on rotor LE plane; 2005 fan rig measurements; 4694 RPM.

with the peak source were removed from the beamforming image. The results after removal, at each frequency, of the main coherent source are shown in Figure 7, where the scale is the same as in Figure 2. It is observed that the 4000 Hz image is "wiped out" almost completely. Hence, all visible sources in that frequency band were apparently coherent. This is surprising, because it is natural to expect that broadband noise sources on stator vanes are incoherent from blade to blade. It looks as if the stator is vibrating as a whole. Since the stator source at 4068 Hz is presumably linked to the rotor source at 2894 Hz, it is also well possible that the rotor was vibrating as a whole. This may indicate a rotor instability.

3.3. INTAKE ARRAY MEASUREMENTS OF 2007

Similar rig measurements were carried out two years later, in 2007. The numbers of rotor blades and stator

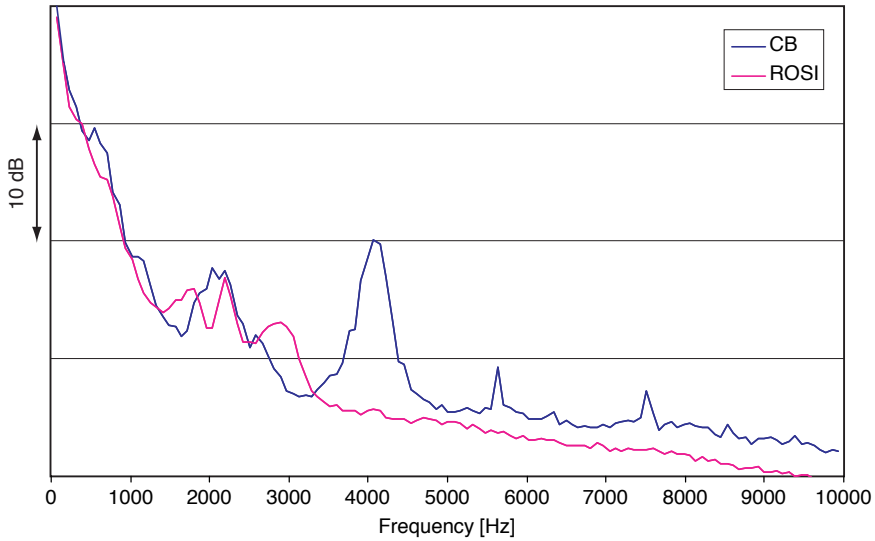

Figure 4: Narrow-band peak values of beamforming with intake array; 2005 fan rig measurements; 4694 RPM.

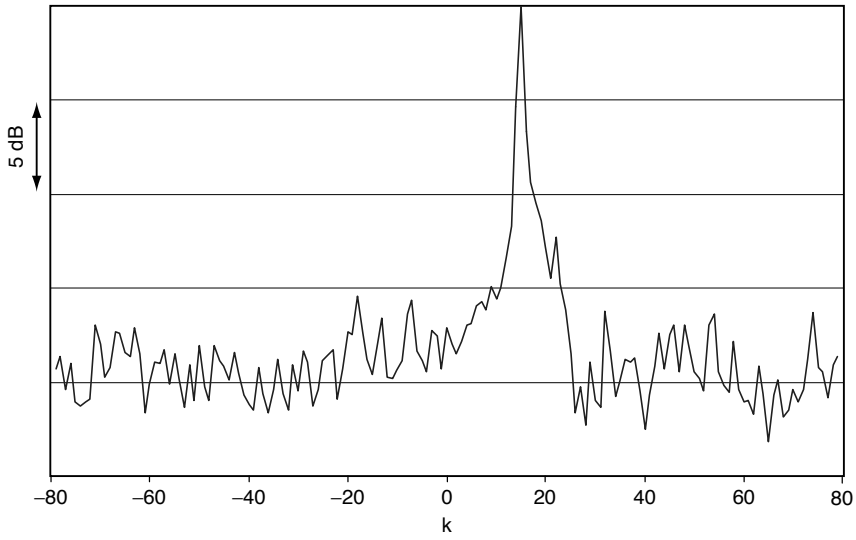

Figure 5: Intake array mode spectrum at 4068 Hz; 2005 fan rig measurements; 4694 RPM.

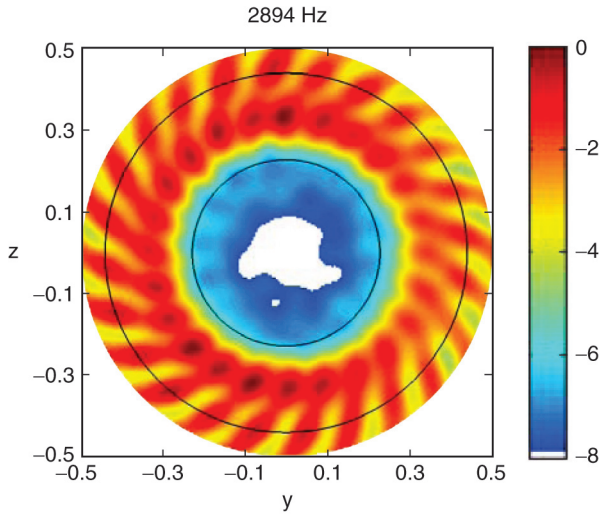

Figure 6: Intake array ROSI image on rotor LE plane; narrow-band result at 2894 Hz; 2005 fan rig measurements; 4694 RPM.

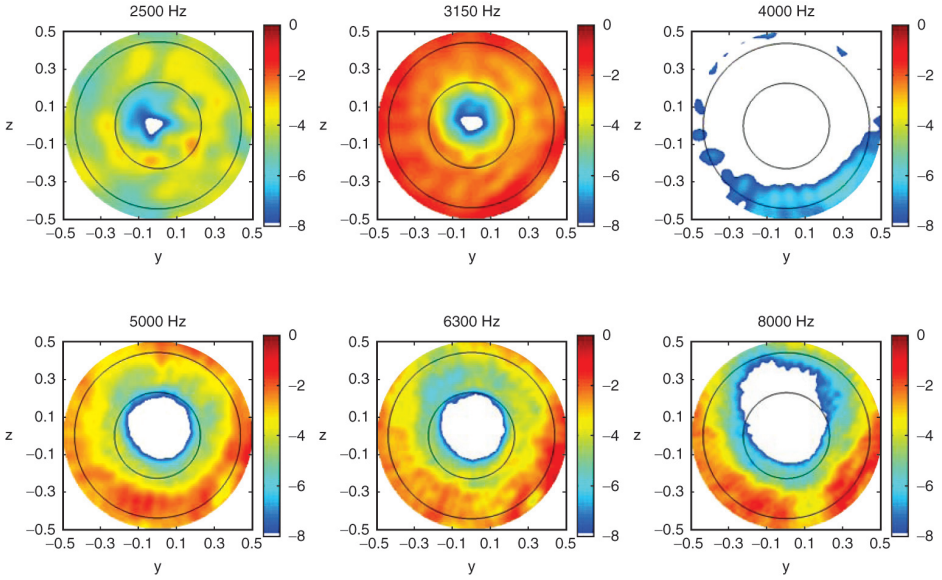

Figure 7: Intake array CB images on stator LE plane; main coherent source components removed using CLEAN-SC; 2005 fan rig measurements; 4694 RPM.

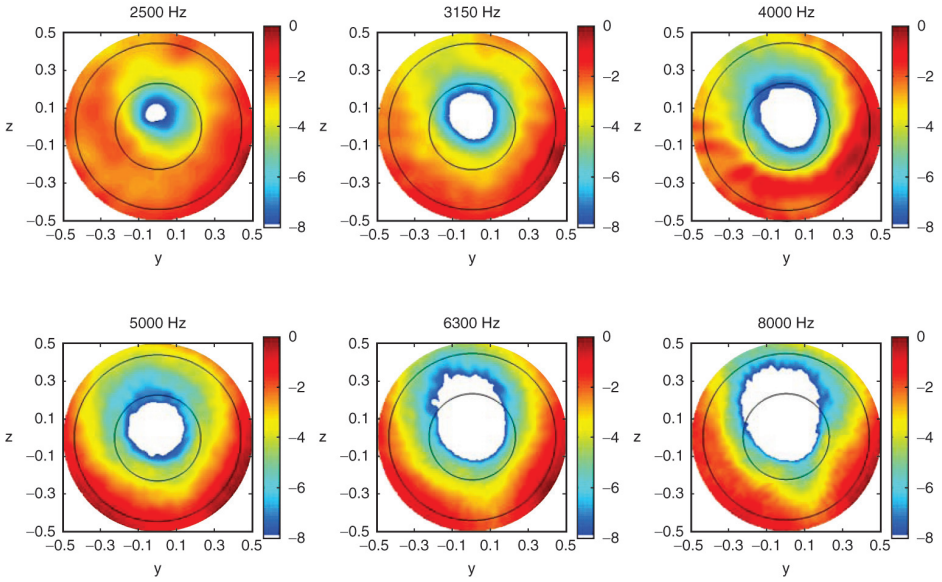

Figure 8: Intake array CB images on stator LE plane; 2007 fan rig measurements; 5049 RPM.

vanes were 20 and 44, respectively. Again, we consider a low shaft speed case: 5049 RPM (55% of the maximum speed). For this case, beamforming provided almost no information about the sources. In the intake CB images (Figure 8) there are no source details visible. The same holds for the ROSI images (Figure 9), except for some vague tip sources at 8000 Hz. Furthermore, application of CLEAN-SC did not reveal dominant extended source areas. As in the previous section, added information could be obtained by considering azimuthal modes. A color plot showing the levels of azimuthal modes at a range of frequencies is shown in Figure 10.

A remarkable feature of Figure 10 is the dominance of positive modes. An obvious explanation is the partial shielding by the rotor of sound that is generated at the stator. Positive modes rotate in the same direction as the rotor,

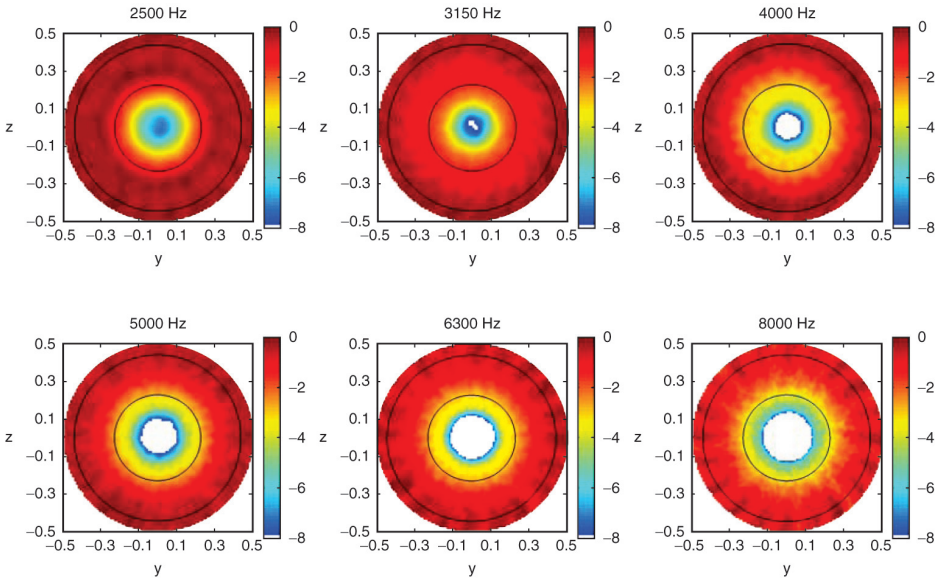

Figure 9: Intake array ROSI images on rotor LE plane; 2007 fan rig measurements; 5049 RPM.

and negative modes are contra-rotating. A thorough mathematical approach that includes rotor transmission effects of fan broadband noise was developed by Hanson[15]. However, it was demonstrated by Schulten[16] that a good first estimate of the actual sound transmission of a duct mode through a rotor can be made using the "Shielded Fraction":

$$S_{k\mu}(r) = \min\left\{1, \frac{B}{2\pi}\left(x_{\mathrm{TE}} - x_{\mathrm{LE}}\right)\left|\frac{2\pi\Omega}{U} + \frac{k}{\mathrm{Re}(\alpha_{k\mu})r^2}\right|\right\}, \quad (18)$$

where:

μ is the radial mode number,

r is the radial position at which an acoustic ray from the source to the receiver intersects the rotor,

B is the number of rotor blades,

x_{TE} is the axial position of the rotor blade LE,

x_{LE} is the axial position of the rotor blade TE,

α_{km} is the axial wave number.

For upstream propagating modes, we have $\mathrm{Re}(\alpha_{km}) < 0$. Therefore, the least shielding and, consequently, the most transmission is expected for $k > 0$.

To verify this shielding effect, the

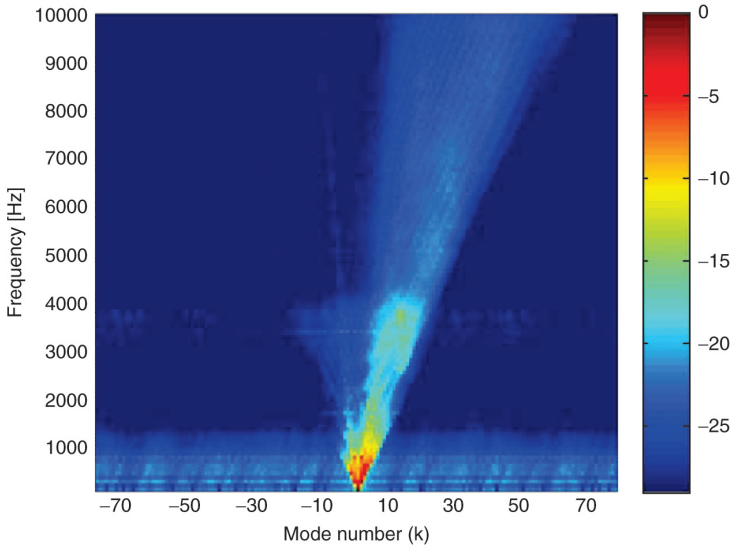

Figure 10: Intake array mode spectra; 2007 fan rig measurements; 5049 RPM.

mode spectra of a synthesized sound field were calculated. An acoustic dipole was modeled at the LE of one of the vanes stator. The radial position was 90% of the tip radius. The sound field of the dipole was obtained by taking a directional derivative of the expression for an acoustic monopole by Rienstra and Tester[17]. This expression is basically a summation of duct modes, and it includes the effects of lining. The dipole was directed perpendicularly to the stator surface, which was assumed to have a local camber angle of 30° at the LE. Transmission through the rotor was incorporated by multiplying the amplitude of each mode with $1–S_{k\mu}(r)$, where r was again at 90% tip radius. The simulated mode spectra are shown in Figure 11, which shows clear resemblance with its measured counterpart, Figure 10.

Another possible explanation for the asymmetry in Figure 10 could have been that the broadband noise sources were rotor-bound. Then, the asymmetry was due to a combination of source rotation and source spectra that decayed with frequency. Simulations with a rotating monopole indeed showed asymmetric mode spectra, with the highest levels at positive k. However, the asymmetry was not as pronounced as in Figure 10. With more realistic simulations, in which the rotating monopoles were replaced by rotating dipoles pointing perpendicularly to the rotor surfaces, the dominance of positive modes was lost.

In summary, these observations made it likely that the broadband noise measured in the intake was generated at the stator.

3.4. BYPASS ARRAY MEASUREMENTS OF 2007

During the 2007 measurement campaign, acoustic data were also measured with the bypass array (see Figure 1). We consider a case at more or less the same condition as in the previous section: 5047 RPM. The CB images of the broadband noise are shown in Figure 12. In a number of frequency bands, we can clearly recognize the 44 stator vanes.

In fact, the results look remarkably good, knowing that:

(a) the duct is annular, so there was no line of sight from each acoustic

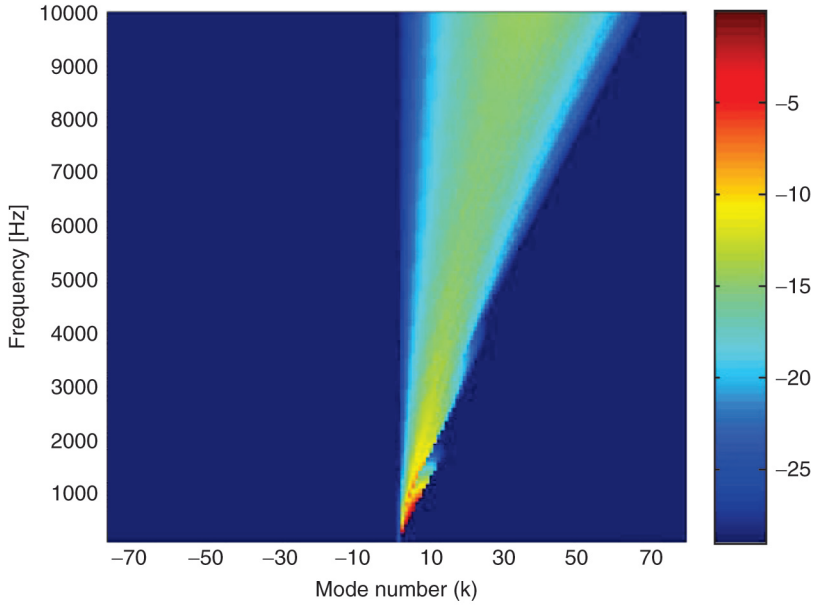

Figure 11: Intake array mode spectra of a stator dipole source at 90% radius; simulation including the effects of liner and rotor shielding; 5049 RPM.

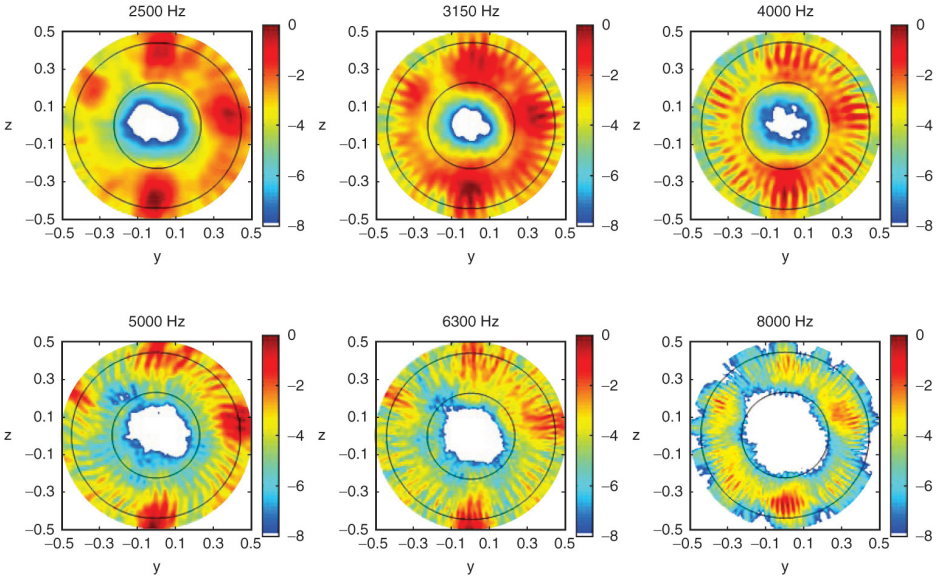

Figure 12: Bypass array CB images on stator TE plane; 2007 fan rig measurements; 5047 RPM.

source to each microphone,

(b) there was no liner between the stator and the bypass array.

Simulations with a hard walled duct showed beamforming images that look significantly worse than the images obtained from the measurements. Maybe, the uniform flow assumption that was used for the simulations was not adequate, and the shear of the flow should be taken into account.

A noticeable feature of the beamforming images is that sound sources seem to be distributed along the span, rather than being concentrated in the tip region. This could mean that sources in the tip region (e.g., due to tip vortices from the rotor) were of minor importance. It is further noted that no large coherent structures in the beamforming images, such as reported in Section 3.2, were found using CLEAN-SC.

Again, added information could be gained from the mode spectra, which are shown in Figure 13. In contrast with

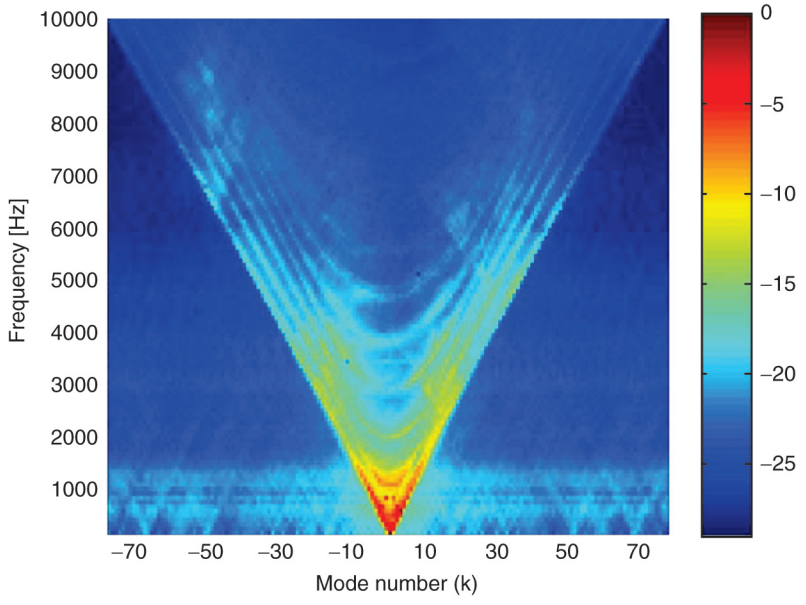

Figure 13: Bypass array mode spectra; 2007 fan rig measurements; 5047 RPM.

the intake mode spectra (Figure 10), there is no preference for positive or negative k. This may indicate that the sound sources were located near the trailing edges of the stator vanes, where the camber angles are small, and, therefore, the dipole-like source directivity does not lead to dominance of positive or negative modes. Dipoles on the stator LE would have led to asymmetry in the mode spectra, though less pronounced than in Figure 10. Similar results of bypass azimuthal mode measurements were reported by Abdelhamid et al[2].

4. CONCLUSIONS

The merits were demonstrated of conventional and advanced beamforming techniques to locate broadband noise sources on the rotor and the stator of a fan rig. Beamforming was applied to measurements with circular arrays in the intake and in the bypass. These arrays are normally used for the detection of azimuthal acoustic duct modes.

With the use of the deconvolution technique CLEAN-SC, some forward radiating broadband noise sources were shown to be coherent over large areas, maybe because of rotor instabilities. With the use of intake azimuthal mode data, it could be made plausible that other forward radiating broadband noise sources originated from the stator.

Beamforming with the bypass array exhibited noise sources on the stator vanes which were distributed along the span, rather than being concentrated in the tip region. In other words, tip noise sources seemed to be of low importance. The bypass mode detection results seemed to indicate that the noise sources were located at the trailing edges of the stator vanes. The good quality of the bypass array beamforming images are not well understood, in view of the fact that the presence of the reflecting wall was not taken into account. Further research is needed to understand this.

ACKNOWLEDGMENTS

The tests were carried out within the EU-funded projects SILENCE(R) and PROBAND. Assystem UK Ltd is acknowledged for providing the fan rig drawing of Figure 1. The author is grateful to Dave Tomlinson (Rolls-Royce UK) for providing details of the rig geometry and the flow conditions. The author thanks Sjoerd Rienstra (TU Eindhoven) for providing his MATLAB script to test the Green's function routine.

REFERENCES

[1] Sijtsma, P., and Stoker, R.W., "Determination of Absolute Contributions of Aircraft Noise Components Using Fly-Over Array Measurements", AIAA Paper 2004-2958, May 2004.

[2] Abdelhamid, Y.A., Ng, L.L., Hanson, D.B., and Zlavog, G., "Fan Broadband Noise Generation and Propagation", AIAA Paper 2006-215, January 2006.

[3] Moreau, A., and Enghardt, L., "Ranking of Fan Broadband Noise Sources Based on an Experimental Parametric Study", AIAA Paper 2009-3222, May 2009.

[4] Mueller, T.J. (Ed.), *Aeroacoustic Measurements*, Springer, 2002.

[5] Sijtsma, P., "Using Phased Array Beamforming to Locate Broadband Noise Sources inside a Turbofan Engine", AARC Engine Noise Phased Array Workshop, Cambridge, MA, 11-12 May 2006.

[6] Sijtsma, P., "Feasibility of In-Duct Beamforming", AIAA Paper 2007-3696, May 2007.

[7] Lowis, C.R., and Joseph, P., "A Focused Beamformer Technique for Separating Rotor

and Stator-Based Broadband Sources", AIAA Paper 2006-2710, May 2006.

[8] Dougherty, R.P., and Walker, B.E., "Virtual Rotating Microphone Imaging of Broadband Fan Noise", AIAA Paper 2009-3121, May 2009.

[9] Sijtsma, P., "CLEAN Based on Spatial Source Coherence", *International Journal of Aeroacoustics*, Vol. 6, No. 4, 2007, pp. 357–374.

[10] Sijtsma, P., Oerlemans, S., and Holthusen, H., "Location of Rotating Sources by Phased Array Measurements", AIAA Paper 2001-2167, May 2001.

[11] Oerlemans, S., Sijtsma, P., and Méndez López, B., "Location and Quantification of Noise Sources on a Wind Turbine", *Journal of Sound and Vibration*, Vol. 299, February 2007, pp. 869–883.

[12] Oerlemans, S., "Location and Quantification of Helicopter Noise Sources in a Wind Tunnel", Proceedings of the 32nd European Rotorcraft Forum, Maastricht, The Netherlands, September 2006.

[13] Rademaker, E.R., Sijtsma, P., and Tester, B.J., "Mode Detection with an Optimised Array in a Model Turbofan Engine Intake at Varying Shaft Speeds", AIAA Paper 2001-2181, May 2001.

[14] Tyler, J.M., and Sofrin, T.G., "Axial Flow Compressor Noise Studies", *SAE Transactions*, Vol. 70, 1962, pp. 309–332.

[15] Hanson, D.B., "Broadband Theory for Coupled Fan Stages Including Blade Row Reflection/Transmission Effects", AIAA Paper 2002-2488. June 2002.

[16] Schulten, J.B.H.M., "Transmission of Sound through a Rotor", DGLR/AIAA 14th Aeroacoustics Conference, Aachen, Germany, 11-14 May 1992.

[17] Rienstra, S.W., and Tester, B.J., "An Analytic Green's Function for a Lined Circular Duct Containing Uniform Mean Flow", AIAA Paper 2005-3020, May 2005.

NEW TIME-DOMAIN ACOUSTIC BEM SOLVER

The latest version of the simulation platform LMS Virtual.Lab Acoustics integrates a powerful time-domain BEM solver developed by IMACS, a spin-off from the Ecole Polytechnique in France. This powerful back-engine lets acoustic engineers perform realistic simulations very efficiently and gain more insight into a wide variety of acoustic issues including for instance engine injection ticks, tire noise and door slams – important brand aspects for the automotive industry. Customers like PSA Peugeot Citroën have been using the time-domain BEM solver technology for several years to efficiently perform powertrain-related acoustic simulations. Denis Thenail of PSA explained, "From very early on, PSA has recognized and supported the time-domain acoustic BEM technology developed by IMACS. For several years now, we have been using this solver for powertrain radiation, exterior vehicle acoustics and a variety of other applications. This solver is extremely efficient and robust enough to solve large BEM models — both from a computation and memory point of view. As such, more cases can be addressed in less time, allowing more iterations to optimize vehicle acoustics. Today, we are glad to benefit from this technology in LMS Virtual.Lab, the simulation platform chosen by PSA." "The latest Rev 9 release of LMS Virtual.Lab Acoustics is in fact our biggest release in twenty years of development, building on LMS SYSNOISE and the previous releases of LMS Virtual.Lab Acoustics. This new robust time-domain BEM is an excellent solver for users dealing with impulsive or wide frequency noise issues. It is designed to handle the most complex models with the highest fidelity and efficiency levels possible. And it perfectly complements our other top-performing solvers like fast multipole BEM (FMBEM) and the FEM PML (Perfectly Matched Layer) technology added to our classic FEM solvers. Many of our OEM customers appreciate the flexibility of being able to work with either highly efficient FEM or BEM solvers – depending on their needs," said Stefaan Goossens, Vice President, Simulation Division, LMS International.